REVIEW ARTICLE

Evaluation of the use of global satellite–gauge and satellite-only precipitation products in stream flow simulations

Hieu Thi Bui[1] · Hiroshi Ishidaira[2] · Ning Shaowei[3]

Abstract

Satellite remote-sensing products with high spatial and time resolution are expected to provide alternative data sources for data-sparse regions. This study clarifies if the satellite–gauge product outperforms the satellite-only product by comparing remote-sensing precipitation products: one that incorporates rain gauge data (GSMaP-Gauge) and one that uses satellite only (GSMaP-MVK). The appropriateness of those two commonly used high-resolution products as the input to the conceptual hydrological model Hydrologiska Byråns Vattenbalansavdelning for stream flow prediction was also investigated. In addition, we also analyzed the deviations of model parameters due to the bias in remote-sensing precipitation inputs compared to standard ground measurements. The results indicated that GSMaP-Gauge was superior, with satisfactory to good performances in predicting stream flow in both temperate and subtropical basins (Hyeonsan, Fuji, and Da). However, its performance was slightly worse than GSMaP-MVK in the Upper-Cau basin, which was explained by the poor quality of the adjusted data source due to sparse data and the satellite–gauge blending algorithm of GSMaP-Gauge. Better parameter agreements with the observations of GSMaP-Gauge than GSMaP-MVK were found in the Hyeonsan and Da river basins where GSMaP-Gauge showed almost consistent relationship of monthly rainfall compared to ground measurements.

Keywords Remote sensing precipitation · Satellite-gauge product · Satellite-only product · Stream-flow simulation · Parameter adjustment

Introduction

Precipitation is one of the most important inputs for hydro-meteorological modeling. However, in many regions of the world, particularly in developing countries, data on rainfall are very poor or even nonexistent due to inadequate funding for the installation and operation of ground-based measurement networks. This problem is a challenging task for hydrology applications, and it bottlenecks the water resources management of these countries. During the last two decades, remote-sensing rainfall estimation products with broad spatial coverage and repeated temporal coverage have provided a potential solution to the lack of data in these regions.

Although satellite-based precipitation products have broad spatial coverage and repeat temporal coverage, satellite rainfall values are just estimates, which have various sources of uncertainty (e.g., gaps in the revisit times, an indirect relationship between remote signals and the rainfall rate, atmospheric effects that modify the radiation field, the coverage of the satellite, and the spatial and temporal sampling discrepancy between satellite estimates and the ground-based estimates). There have been many efforts to improve the pure satellite precipitation products by incorporating rain gauge information in satellite-based rainfall retrieval algorithms, with the emergence of global satellite–gauge rainfall estimation products such as Gage Adjusted Global Satellite Mapping of Precipitation (GSMaP-Gauge), adjusted Precipitation Estimation from Remotely sensed information Using Artificial Neural Network (PERSIANN) (Hsu et al.

✉ Hieu Thi Bui
   buihieudhxd@gmail.com

1   Department of Environmental Engineering, National University of Civil Engineering, 55 Giai Phong Road, Hanoi, Vietnam

2   Department of Civil and Earth Resources Engineering, International Research Center for River Basin Environment (ICRE), University of Yamanashi, Takeda 4-3-11, Kofu, Yamanashi 400-8511, Japan

3   College of Civil Engineering, Hefei University of Technology, 193 Tunxi Road, Hefei, China

1997), and Multi-Satellite Precipitation Analysis (TMPA) (Huffman et al. 2007). This raises two questions. The first is whether the satellite–gauge precipitation products always outperform the original satellite-only precipitation products. The second is whether high-resolution satellite-based precipitation estimates can provide reliable rainfall information for discharge predictions. This study evaluated and compared two global remote-sensing precipitation products: GSMaP-Gauge and Global Satellite Mapping of Precipitation moving vector with Kalman filter (GSMaP-MVK). They were developed as Global Satellite Mapping of Precipitation (GSMaP) projects, which promote high precision and high resolution from not only microwave radiometers but also geostationary infrared radiometers. There are several reasons for choosing these two products. First, they produce a very high spatial resolution (0.1°) and high time resolution (1 h). In addition, the GSMaP-MVK product has been successfully producing fairly good pictures in near real time and has a comparable score compared to other high-resolution systems (Ushio et al. 2009). However, GSMaP-MVK has a tendency to underestimate extremely high precipitation rates compared to the ground measurements in some particular operational applications (Ushio et al. 2013). In this circumstance, GSMaP-Gauge has been developed to fill the gap in the precipitation estimates between the satellite and rain gauge data attributable to the difference in spatial and temporal resolution.

It is important to investigate remote-sensing precipitation products in various areas and different climate regimes to obtain a more comprehensive understanding of them, which is useful for improving not only products themselves but also the utilization of the data that they provide. Several previous studies have assessed the stream flow prediction capability of different remote-sensing products (Stisen and Sandholt 2010; Bitew and Gebremichael 2010; Shrestha et al. 2008; Liu et al. 2017). It is concluded that satellite rainfall products are potential precipitation input for hydrological applications; performance of hydrologic model depends on satellite product type, watershed size, and hydroclimatic region (Su et al. 2007; Tobin and Bennett 2009; Yilmaz et al. 2005).

The studies of satellite rainfall products through stream flow simulation in hydrological modeling framework are few in number and do not cover adequately different satellite rainfall products, basin sizes (particularly small basins), and hydroclimatic regions (Bitew et al. 2012). This study provides well-organized and synthesized insight into the hydrological applications of some remote-sensing precipitation estimations in several river basins of various sizes and under different climates. We examined the effectiveness of combining rain gauge measurements with a satellite-only product and investigated the ability and shortcomings of remote-sensing precipitation products as an input into a hydrological model for stream flow prediction in several river basins in East and Southeast Asia under a wide range of climate conditions and topographical terrains with different degrees of complexity. In addition, we analyzed the deviations of model parameters due to the bias in remote-sensing precipitation inputs compared to standard ground measurements.

Study area and materials

Study area

We included basins in a wide range of latitudes and under different climatic conditions (tropical monsoon and temperate climate) in three different Asian countries (Japan, Vietnam, and South Korea). The Hyeonsan and Fuji basins are located in mid-latitude areas of South Korea and Japan, respectively, and they have relatively dense rain gauge networks. On the other hand, the Da and Upper-Cau river basins are located in the northern part of Vietnam in a tropical climate area, and they have much lower rainfall gauge densities. The local dense rain gauge networks (Table 1) in 4 investigated river basins are used as reference data to evaluate the performance of remote-sensing precipitation products.

Da river basin is a humid catchment (annual relative humidity of 82%; 85–90% in the rainy season) and is the biggest branch of the Red river basin, which is located in a

Table 1 Summary of characteristics of the study basins

	Fuji	Da	Upper-Cau	Hyeonsan
Country	JP	VN	VN	SK
Area (km^2)	2179	45,900	2760	1167
Size classification*	Medium	Large	Medium	Small
Gauge number	19	22	8	14
Spatial extensions	35.5N–36N	20.5N–25N	11N–14N	21.5N–22.1N
	138E−139E	100E−106E	105E−106E	128E−130E

JP, Japan; *VN*, Vietnam; *SK*, South Korea

*The large, medium, and small size rivers basins are with total area of > 20,000, 2000–20,000, and < 2000 km^2, respectively (Kendale 2011)

2 Springer

diverse and complex topographical area, characterized by linear belt-shaped, strongly folded bedrock. The regional relief is strongly dissected with relative height differences from 1500–2000 m to 30–50 m, changing alternately from high mountain ranges surrounding plateaus to low mountains with valleys. Its climate is tropical monsoonal with two different seasons: a warm and humid summer, and cool and dry winter. Rainfall is distributed unevenly over the catchment, both in time and in space, which is attributed to many factors such as the elevation of the topography and the orientation of mountains. The high mountains in the Pusilang mountain chain block the southwest monsoon that causes high rainfall on the east side of the basin. The annual rainfall in the Hoang Lien Son mountain chain, which includes many high mountains (above 2800 m), is very large, from 2000 to 3200 mm per year. Meanwhile, the west side of the Da river basin is sheltered from the wind, which results in a lower annual rainfall, from 1800 to 2000 mm in Muong Nhe Province and 1200–1600 mm in the Son La and Moc Chau plateaus. Da river basin consists of different rock types including terrigenous rocks, carbonate rocks (mainly limestone and dolomite), and metamorphic siliceous rocks. There are plentiful types of soil in the basin due to the effects of internal radiation regime with abundant tropical heat and light energy, high humidity climate, rich rain, and heavy rains: wet soil, semi-flood soil, alluvial rivers and streams, accumulations valley soil, degenerated clay by paddy change, clay typical soil, clay humus soil on the mountain, inert limestone soil, and stone. The major soil types of Da river basin are clay typical soil and clay humus soil on the mountain, which account for 51.47% and 41.23% of the total area of the river basin, respectively. Land cover types of Da river basin can be classified into three types: annual crops, long-term crop, and forest vegetation. The vegetation in the mountains northeast is plentiful, and the forest area is about 28.25% of the natural area in 2000 subtropical climate region with two distinct seasons. The rainy season, which provides more than 80% of the total annual rainfall, usually starts in May and ends in September. The topography of the Upper-Cau river basin includes mountainous areas, with only a few mountain peaks exceeding 1000 m and hilly land that is much less complicated than the Da river basin. As a result of the less complex topography, the spatial distribution of rainfall there is more even than in the Da river basin, with the average annual rainfall varying from 1500 to 2000 mm per year. The major soil groups of Upper-Cau river basin are rocky–inert erosion, boggy and slope convergent, yellow red, and mountainous red yellow humus (Thai et al. 2017). Land cover over Upper-Cau river basin is diverse including fruit tree, scrub mixed with woods, grass mixed with farm land, long-term industrial plantation, irrigated rice, subsidiary and short industrial, crops, rice and subsidiary crops, burn over land, grass, rich and medium natural forest, poor natural forest, residential land, scrub, brushwood (Jayawardena et al. 2002).

Fuji River is located in central Japan; it originates in the Southern Alps and is surrounded by many high mountains in the west (peaks over 3000 m) and north (peaks over 2000 m). The geological features of the basin are very steep, with 90% of the area covered by mountains. Due to a giant dislocation called the Itoi river-Shizuoka Tectonic Line, which runs in a north–south direction, along with many other dislocations in the region that have caused many collapsed areas, the geological features are very complex and fragile. Therefore, the spatial rainfall pattern varies significantly. Annual rainfall in the Kofu basin is as low as 1100 mm. The middle and lower reaches experience more precipitation, with high average values ranging from 2000 to 2500 mm. The whole basin receives a mean annual precipitation of around 2100 mm. The basin lies in an inland mid-latitude climate region with hot and humid summers, and cold and dry winters. The temperature differences between summer and winter are extreme, with average temperatures of 26 °C and 3 °C, respectively. A geologic map of Fuji river basin with distribution of major rock types including quaternary, mesozoic, volcanic rock, plutonic rock can be found in catalogue of rivers for Southeast Asia and the Pacific (Jayawardena et al. 1997). The land use of Fuji river basin includes built-up area, paddy field, cultivated area, orchard, mulberry field, tea field, forest, shrubland and grassland, barren land (Jayawardena et al. 1997) (Fig. 1).

The drainage area covers the Upper-Cau river basin to the gauging station Gia Bay in Thai Nguyen, with a drainage area of 2760 km^2. As with the Da river basin, it is located in a humid,

The Hyeongsan River flows through the southeastern part of Gyeongbuk Province on the Korean Peninsula. It covers an area of 1160.80 km^2 and consists of low mountainous relief, the highest peak being 901 m (Mt. Beakwoon) in the upper stream; there is a plain in the lower stream. The average annual precipitation over the river basin is approximately 1117 mm, with a moderate spatial distribution of 1000 to 1700 mm. The major rock types over Hyeonsan river basin include bulguksa granite, yucheon group, hayang group, sedimentary rocks (Jayawardena et al. 2012). The land use of this basin is classified into 6 main groups including water, urban, grassland, forest, paddy field, and agricultural field (Jayawardena et al. 2012). The major soil type of Hyeonsan river basin is Hayang group, and the major land cover type is forest.

Fig. 1 **a** Locations of targeted
river basins (red points) and rain
gauges, stream-flow gauges of
b Da river basin **c** Upper-Cau
d Fuji river basin **e** Hyeonsan
river basin
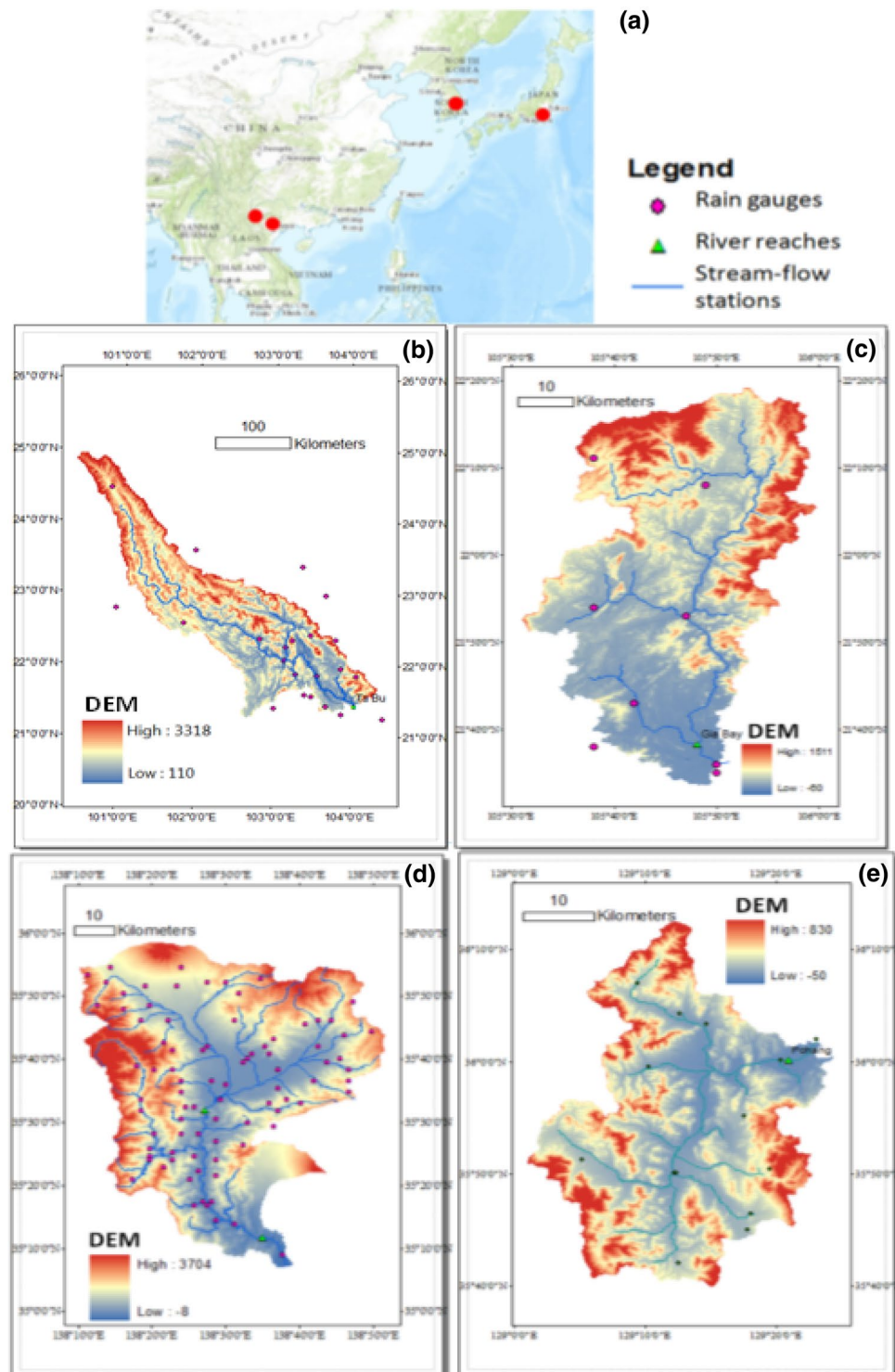
Remote-sensing precipitation products

GSMaP-MVK

GSMaP-MVK version 5.222.1 was used in this research. The GSMaP-MVK method estimates the precipitation rate from microwave (MW) sources and uses the morphing method (Joyce et al. 2004) to produce a morphed product. Surface rain rates in 0.1° pixels of the infrared (IR) brightness temperature were obtained using a Kalman filter. The rainfall predictions were refined based on the relationship between the IR brightness temperature and the

surface rainfall rate. The microwave radiometer (MWR) sensors used for GSMaP-MVK rainfall retrieval include the Special Sensor Microwave/Imager (SSM/I), TRMM Microwave Imager (TMI), and Advanced Microwave Scanning Radiometer for EOS (AMSR-E). The IR datasets used for GSMaP-MVK retrieval were supplied from the National Oceanic and Atmospheric Administration (NOAA) Climate Prediction Center (CPC) with 30 min temporal resolution. The latitudinal range of the IR data was 60°N–60°S.

GSMaP-Gauge

This study utilized GSMaP-Gauge version 5.222.1.40. GSMaP-Gauge is a product that is adjusted to the GSMaP-MVK and has been developed to mitigate the mismatches between the ground measurements with the GSMaP-MVK. The gauge-adjusted data sources used in GSMaP-Gauge are the CPC global gauge datasets. It is a unified precipitation product combining all information sources available at the CPC by taking advantage of the optimal interpolation objective analysis technique. The dataset provides daily gauge-based global precipitation with $0.5° \times 0.5°$ spatial resolution. The analysis quality of the CPC dataset varies with the gauge network density. This will consequently have an impact on the quality of GSMaP-Gauge data.

Hydrological model and simulation setups

The HBV model is a conceptual model of catchment hydrology, which simulates discharge with areal mean precipitation as the main input. The HBV model has been used in numerous studies and has been adopted as a standard forecasting tool in nearly 200 basins throughout Scandinavia, with further applications in more than 40 countries. Therefore, we chose to use it in this study. It is characterized by a relatively simple and robust two-layer tank model structure and focuses on capturing the most important runoff generating process. The snow routine, soil and evaporation routine, and groundwater and its response are the three main modules of the HBV model (Fig. 2). The precipitation from rainfall and snow melt computed in the snow routine is transferred into storage in the soil moisture zone through the soil moisture routine. The response routine consists of two interconnected reservoirs. The upper storage zone is fed with water from the soil moisture zone. When available, water percolates from the upper to the lower storage zone at a constant rate. There is runoff from these two storage zones in proportion to their contents. The lower zone is also directly affected by precipitation and potential evaporation in parts that represent lakes, rivers, and outflow areas. Finally, the discharges from the two reservoirs are combined and a simple time–area transformation is applied. This transformation is
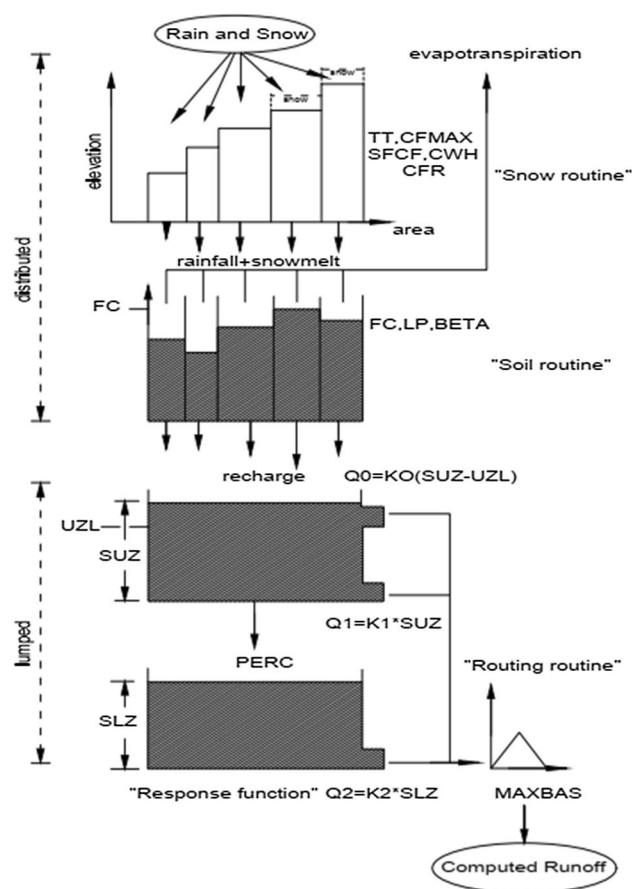

Fig. 2 Structure of HBV model (Seibert 2005)

a triangular function adjusted for the correct timing of peak flows. In this study, given that all four targeted river basins are free of snow, the number of calibrated parameters was decreased from 12 to 9. These calibrated parameters, which determine the soil moisture accounting routine, and the river routing and response routine, are described in Table 2, with their ranges used for automatic calibration and Monte Carlo simulations. The soil moisture routine is controlled by three parameters, denoted as the maximum soil moisture storage FC (mm); soil moisture threshold LP (−), above which actual evaporation reaches potential evaporation; and the parameter BETA (−), which determines the relative contribution of rainfall or snow melt to runoff. The response routine is a lumped model with two boxes connected in series under constant percolation PERC (mm/d). The response function transforms the recharge from precipitation into runoff by simply summing the recharges from the groundwater boxes assumed in the model structure. K_0, K_1, and K_2 are recession coefficients, while a threshold parameter, UZL (mm), is used to produce overflow when the water storage of the upper zone is exceeded. For the routing routine, the generated runoff in one time step is distributed on the following days using

Table 2 Calibrated HBV parameters and their ranges

Parameter	Explanations	Minimum	Maximum	Unit
Soil and evaporation routine				
FC	Maximum soil moisture	50	1000	mm
LP	Soil moisture threshold for reduction in evaporation.	0.3	1	–
BETA	Shape of coefficient	1	6	–
Groundwater and response routine				
K_0	Recession coefficient	0.05	0.5	d^{-1}
K_1	Recession coefficient	0.01	0.3	d^{-1}
K_2	Recession coefficient	0.001	0.1	d^{-1}
UZL	Threshold for K_0 outflow	0	100	mm
PERC	Maximal flow from upper to lower Groundwater box	0	6	
MAXBAS	Routing, length of weighting function	1	5	d

one free parameter, MAXBAS (d), which determines the base of an equilateral triangular weighting function. Six of the calibrated parameters play important roles in determining the discharge quantity predictions: two control the soil and evaporation routine (FC and BETA), three are recession coefficients (K_0, K_1, and K_2), and UZL controls the amount of runoff from the upper and lower reservoirs. Therefore, in this application, the readjustment of model parameters to compensate for the differences in runoff from input rainfall estimates is focused on those six parameters. The role of FC is very important in separating the effective precipitation into runoff and soil moisture. Low FC values indicate a low water holding capacity of the soil and a small amount of water available for evapotranspiration; this in turn enlarges the runoff. BETA controls the partition of the precipitation into runoff and soil moisture recharge. Low BETA values indicate more runoff formation than soil moisture recharge (Nibret et al. 2010). While K_0 and K_1 affect the overland flow and quick interflow, K_2 has an impact on base flow from deep groundwater. Larger values of these recession coefficients result in an increasing outflow at the catchment outlet. In addition, UZL also affects the runoff from the upper zone layer box. A lower UZL leads to more runoff and vice versa.

Xu and Vandewiele (1994) examined the sensitivity of a monthly rainfall–runoff (RR) model due to errors in rainfall and concluded that watershed models are able to adjust the parameters to compensate for the bias in rainfall. Therefore, the quantitative bias of different remote-sensing precipitation inputs would cause a difference in calibrated model parameters. Therefore, the discrepancy of the rainfall inputs is compensated for by changing the parameters to maintain the simulated discharge as well as possible. To assess the relationship between model parameters obtained from rain gauge data and satellite-derived data, it is vital to evaluate the population of a parameter set rather than judging a single parameter set because of "equifinality" issues. This problem states that there is no unique solution for the hydrological model calibration; in other words, equally good

model performances can be obtained from different parameter sets. The assessment of model parameter uncertainty is beyond the scope of this study; however, a parameter population containing 10,000 model parameter sets was generated using a Monte Carlo algorithm for analyzing the impact of an inaccurate amount of remotely sensed precipitation on the reaction of a model parameter that directly affects the outflow at the outlet of a catchment. Only parameter sets that are capable of generating a model performance index with a Nash–Sutcliffe (N–S) efficiency larger than 60% for the best performances by the corresponding rainfall input obtained by the GAP automatic calibration process were kept for analysis. The magnitude of the six parameters referred to earlier was judged graphically using box plots.

The HBV model parameters for each watershed and rainfall input were calibrated separately with different precipitation inputs (local ground rainfall measurements, GSMaP-MVK and GSMaP-Gauge) over the 2-year period of 2002–2003 using automatic calibration by the GAP optimization tools facilitated in the model package. Stream flow was simulated for the validation period of 2004–2005 from the HBV rainfall input for each rainfall source (including local rain gauge data, GSMaP-MVK and GSMaP-Gauge) and the corresponding model parameters. The objective function was to maximize the N–S efficiency between the simulated and observed stream flows. The N–S efficiency and coefficient of determination (R^2) were used to judge the stream flow prediction capability of the alternative rainfall inputs.

Results

Remote-sensing precipitation estimations

Before simulating the daily stream flow predictions of the different rainfall input sources using the HBV conceptual rainfall runoff model, we evaluated the basin average

precipitation forcing input during the calibration period for several criteria: accumulated precipitation, seasonal variation, RMSE, and BIAS. The evaluation of rainfall estimations and stream flow prediction capability of the two GSMaP products are discussed in this section.

Evaluation of the performance of GSMaP-MVK

This section discusses the effects of climate and topography on the performance of the satellite-only precipitation product GSMaP-MVK. Both microwave radiometer in LEO and infrared radiometer in GEO are used to produce the global precipitation map with 1 h and 0.1 degree resolution. GSMaP-MVK applies the algorithm described in Aonashi et al. (1996) and Kubota et al. (2007) to convert the brightness temperature of primary microwave radiometer to surface rain rate. MW sensors measure the MW radiation during the formation of rainfall droplets and thus provide more accurate rainfall estimations than the infrared radiometer. However, they are only available on low-orbit satellites and have a coarse spatial resolution. Another restriction is that they may misclassify very cold surfaces and ice on mountain tops with rain clouds (Dinku et al. 2010). In addition, the overland underestimation of warm orographic rain that does not contain ice particles is also challenging for MW rainfall retrieval, mainly due to ice scattering (Dinku et al. 2010). The precipitation estimates between the microwave overpasses are interpolated using the IR data by the technique of Kalman filter and moving vector, which is described in Ushio et al. (2013).

Our study area contained two different climatic regions. The Hyeonsan and Fuji river basins are located in a temperate zone, whereas the Da and Upper-Cau river basins are in a subtropical zone. All four basins are located in mountainous

areas associated with orographic rainfall. Lifting the moist air for orographic cloud formation may lead to precipitation when the cloud top is still warm and while there is little development of ice particles, which is undetected by the cloud top IR and passive MW (PMW) algorithms. Orographic rainfall could be one factor leading to the underestimation of GSMaP-MVK in our study area along with the small available number of PMW image samplings used for GSMaP-MVK retrieval.

For the mid-latitude river basins, GSMaP-MVK significantly underestimated the rainfall accumulation (Fig. 3) during the two-calibration-year period in both the Hyeonsan and Fuji river basins. In addition to the reasons for rainfall underprediction mentioned above, this can be partly explained by the errors in differentiating between an ice surface and cloud in the ice surface snow screening process of the MW algorithm. In Hyeonsan, although GSMaP-MVK consistently underestimated the rainfall quantity throughout the year, with rainfall under-predictions exaggerated from May to September (Fig. 4), it was able to capture the variation in the monthly rainfall budget during the rainy season. In the Fuji river basin, GSMaP-MVK underestimated the amount of precipitation throughout the year, except in May and June (Fig. 4). The monthly variation in the rainfall budget in Fuji was more similar to observations than in Hyeonsan (Fig. 4). With regard to the second category, GSMaP-MVK rainfall estimations were dramatically lower than the observations during the whole year in the Da river basin. In the Upper-Cau river basin, GSMaP-MVK rainfall accumulation followed the observations quite well, with a marginal overestimation from mid-2002 to mid-2003. This was the result of compensating for the dramatic overestimation in June and relatively moderate under-prediction from August to the end of the year. It is interesting that GSMaP-MVK was able to

Fig. 3 Accumulated precipitation of GSMaP-MVK (red line) and GSMaP-Gauge (blue line) vs ground measurements (green line) in **a** Hyeonsan basin, **b** Fuji basin, **c** Da basin, and **d** Upper-Cau basin
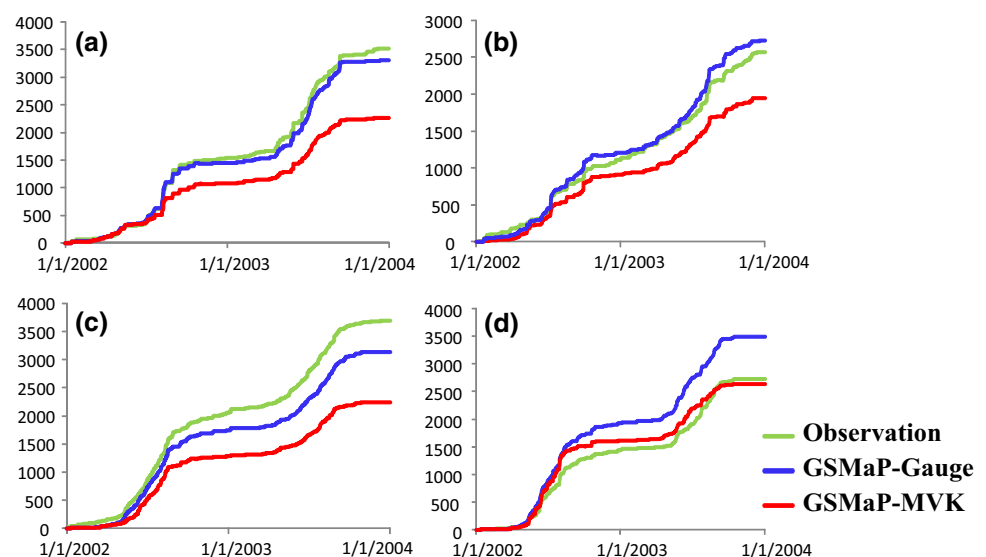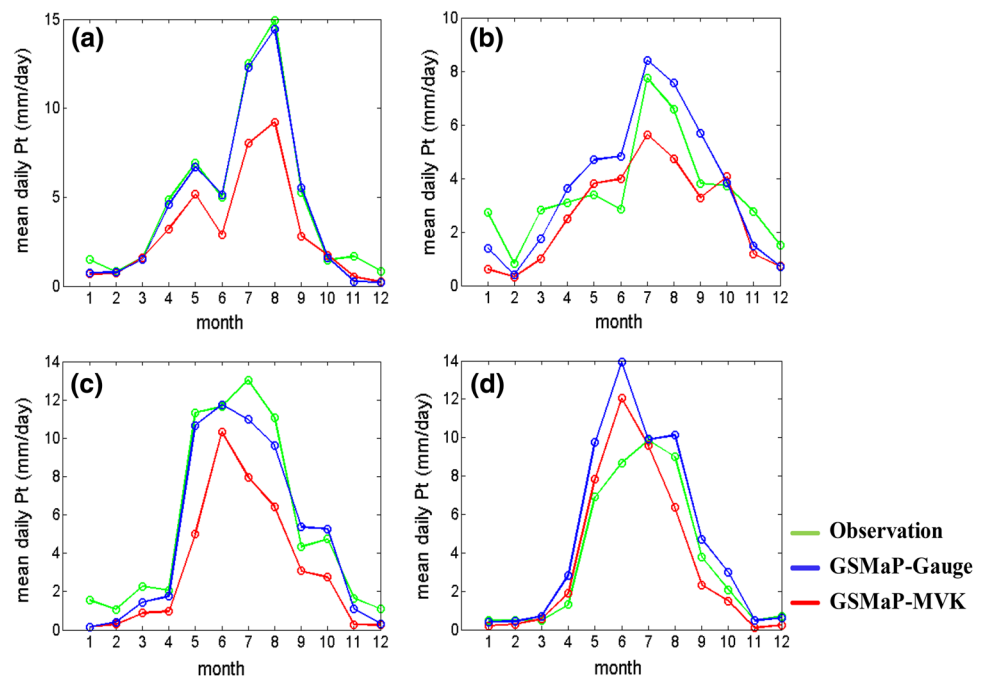
Fig. 4 Seasonal Variation in basin average precipitation of GSMaP-MVK (red line) and GSMaP-Gauge (blue line) vs ground measurements (green line) in **a** Hyeonsan basin, **b** Fuji basin, **c** Da basin, and **d** Upper-Cau basin

produce monthly rainfall fluctuations that were quite close to the ground measurements from the beginning of the year to May. In general, GSMaP-MVK performed better in terms of accumulating the precipitation budget in the Upper-Cau river basin than in the Da river basin.

GSMaP-MVK versus GSMaP-Gauge

In all four river basins, GSMaP-Gauge adjusted the precipitation quality by increasing the amount of precipitation. GSMaP-Gauge gave a very good correction for GSMaP-MVK in Hyeonsan, providing good agreements with rain gauge data for rainfall accumulation (Fig. 3) and monthly variation in rainfall during the wet season (Fig. 4). In the Fuji river basin, although GSMaP-Gauge accumulations were similar to the observations and produced less underestimation during the dry period, it exceeded the rain gauge data during the rainy season. As a result of enlarging the GSMaP-MVK estimations, GSMaP-Gauge produced less underestimation in precipitation accumulation and monthly rainfall budget in the Da river basin. On the other hand, GSMaP-Gauge accumulations notably overestimated reference rain

gauge data by exaggerating the rainfall amount in May and June.

Table 3 shows that in the small and medium size river basin, GSMaP-Gauge with the combination of the rain gauge data expressed a better relationship with the rainfall observations in Hyeonsan, Fuji than Upper-Cau river basin. In Hyeonsan and Fuji, GSMaP-Gauge showed significant improvement compared with GSMaP-MVK with a great reduction in the RMSE and BIAS values. In addition, in the Upper-Cau river basin, GSMaP-Gauge worsened the agreement between GSMaP-MVK and the ground data by drastically increasing the RMSE and BIAS from 2.24 to 39.88 mm/day and from 0.06 to − 1.04 mm/day, respectively. These results indicate that blending remote-sensing precipitation data with rain gauge data do not always lead to better precipitation estimations. One of the reasons could be that there is no rain gauge used to produce CPC global rain gauge data in Upper-Cau basin (Fig. 5). Because the number of the rain gauge of CPC global gauge data in Hyeonsan and Fuji is more than that in Upper-Cau (Fig. 5), the relationship between local rain gauge data and CPC global gauge data in Hyeonsan and Fuji is stronger

Table 3 Relationship between daily average precipitation over catchments between satellite-based precipitation and ground observations using statistics

	RMSE		BIAS	
	GSMaP-MVK	GSMaP-GAUGE	GSMaP-MVK	GSMaP-GAUGE
Hyeonsan	45.79	5.478	1.19	− 0.143
Fuji	28.50	12.63	0.75	− 0.327
Da	71.97	20.67	1.18	0.62
Upper-Cau	2.24	39.88	0.06	− 1.04

Fig. 5 Ground rain gauge distributions of the CPC global gauge data set in the study regions
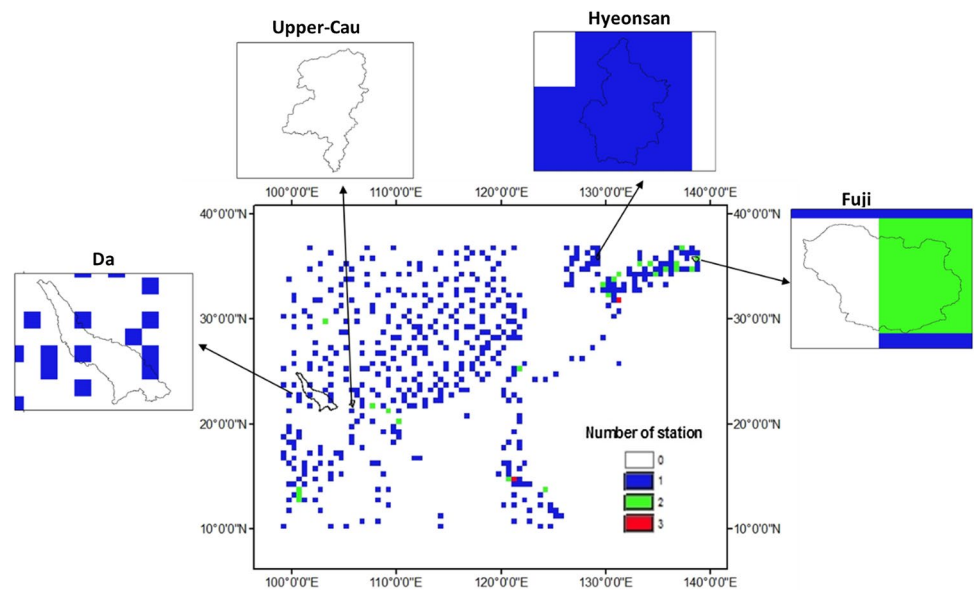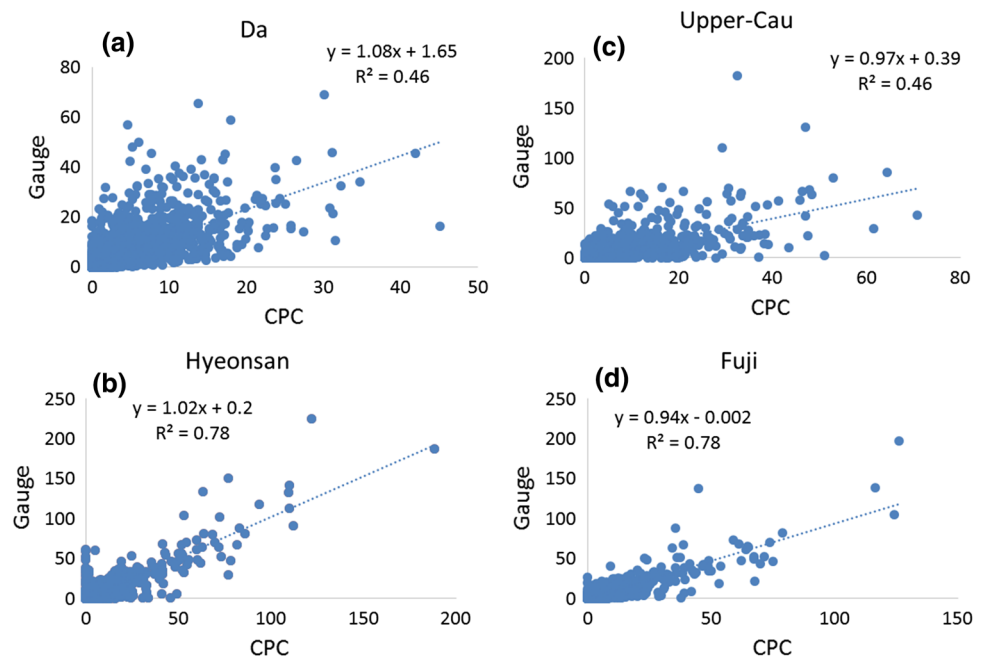

Fig. 6 Relationship between local rain gauge data and CPC global gauge data set in **a** Da, **b** Upper-Cau, **c** Hyeonsan, **d** Fuji

than in Upper-Cau (Fig. 6). Thus, there was significant improvement in GSMaP-Gauge compared with GSMaP-MVK in the Hyeonsan and Fuji basins, but the deterioration of GSMaP-Gauge compared with GSMaP-MVK in the Upper-Cau basin. Therefore, this result highlights that the constraints of the relevant rain gauge density for blending space-born precipitation and ground measurements of rainfall should be implemented in the merging algorithm, to avoid exaggerating the uncertainties due to data sparsity

issues. In addition, there are few "one rain gauge" pixels falling inside the area of Da RB, which results in similar poor relationship between local rain gauge and CPC rain gauge data set in Da to the case of Upper-Cau with the 0.46 R^2 values. However, GSMaP-Gauge was superior to GSMaP-MVK with the RMSE and BIAS from 71.97 to 20.67 mm/day and from 1.18 to 0.62 mm/day, respectively. The huge size of Da river basin would be one factor that mitigates the impact of rain gauge limitation on the quality of satellite–gauge merging precipitation GSMaP-gauge.

Fig. 7 Box plots of 6 parameters impacting on generating discharge for calibration period 2002–2003 in Hyeonsan river basin
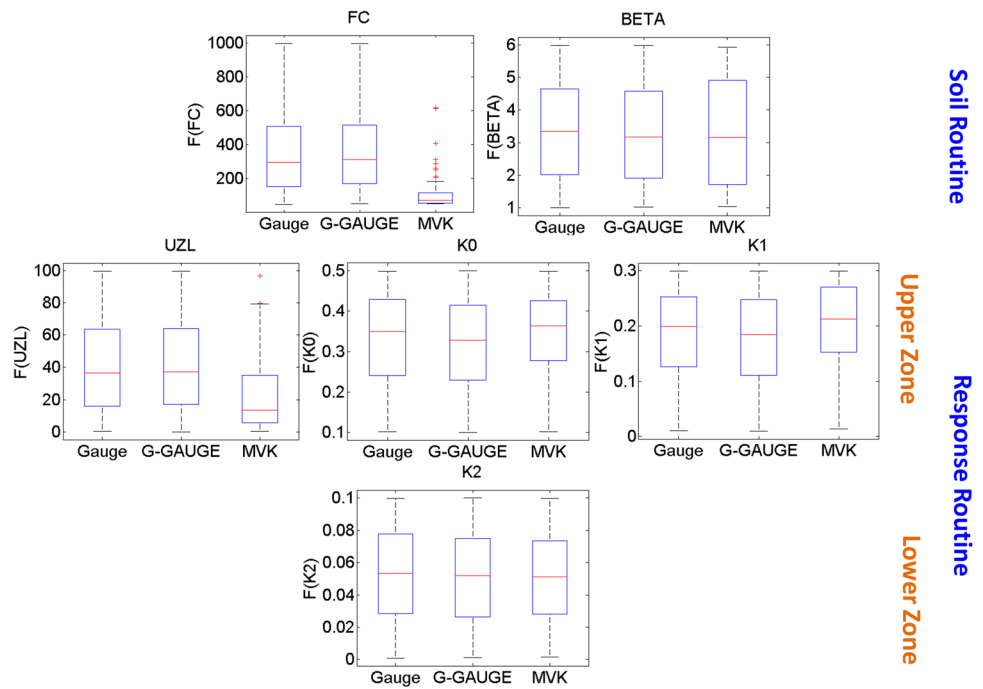
Deviations of model parameters

In the Hyeonsan and Da catchments, because GSMaP-MVK significantly underestimates the accumulation of rainfall and monthly rainfall quantity, the parameters were adapted in a way that the model produced more stream flow. The adjustment of the parameters due to the incorrect estimations of the amount of rainfall was clear in both the soil routine and upper zone and lower zone response

routine in Hyeonsan, with noticeably low GSMaP-MVK's FC, and UZL values and substantially high K_1 values (Fig. 7). Although the adaptation of the parameters was obvious in the soil routine and lower zone response routine in Da river basin, minor differences were seen in the parameters controlling the upper zone (Fig. 8). As a consequence of the dramatic water budget improvement in GSMaP-Gauge compared to the original satellite-only product GSMaP-MVK in these two river basins (Figs. 3

Fig. 8 Box plots of 6 parameters impacting on generating discharge for calibration period 2002–2003 in Da river basin
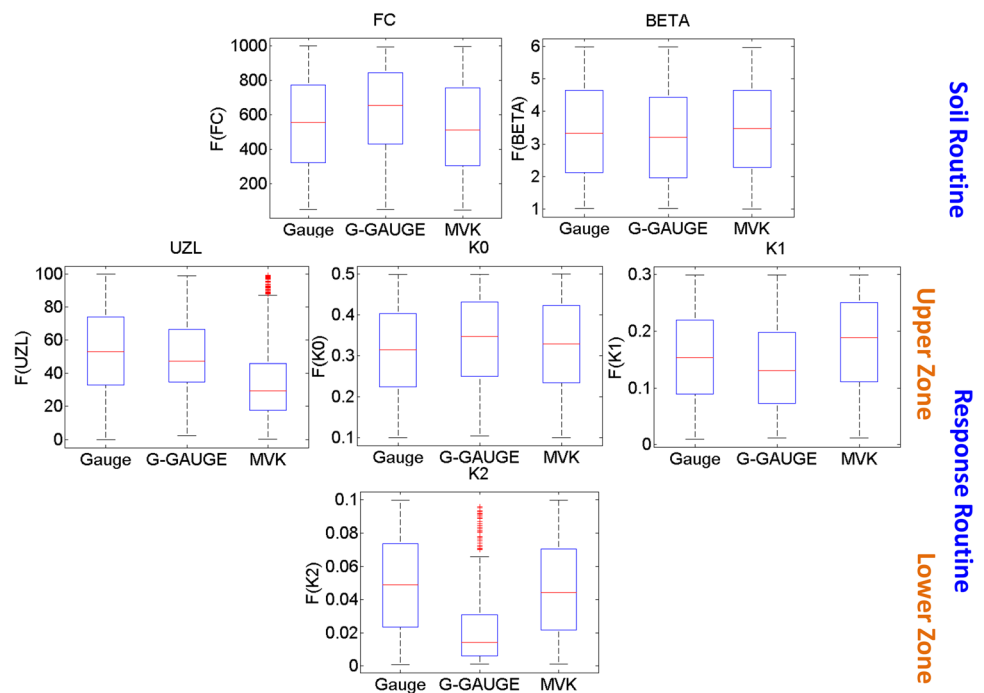
 Springer
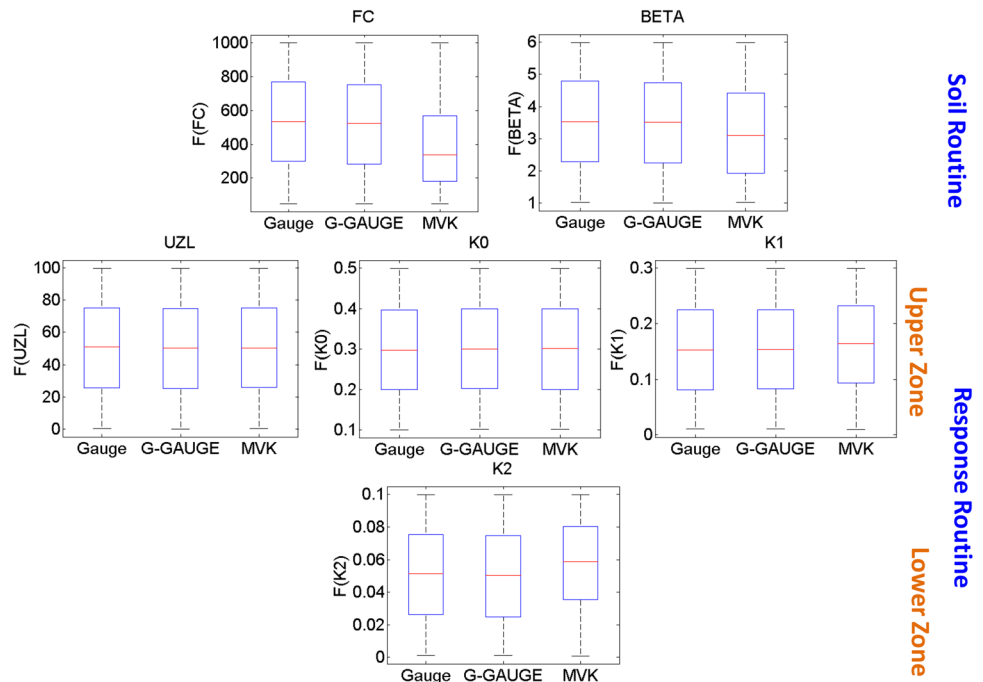
Fig. 9 Box plots of 6 parameters impacting on generating discharge for calibration period 2002–2003 in Fuji river basin

and 4), all six parameters calibrated using GSMaP-Gauge expressed little statistical difference with those obtained from reference rain gauge data.

In the Fuji river basin, although GSMaP-Gauge accumulations deviated slightly from observations, the monthly amounts of rainfall were not consistently underestimated with the larger rainfall budget during the rainy season and the lower precipitation during the dry season compared to the rain gauge data (Fig. 4). This could be one of the reasons for the much less similar quartile ranges of GSMaP-Gauge parameters compared to observations in the Hyeonsan and Da river basins (Fig. 9). In addition, because of the large underestimations of precipitation, GSMaP-MVK generated noticeably low UZL and moderately higher K_1 values, to increase the recharge amount from upper zone box (Fig. 9).

In the Upper-Cau river basin, GSMaP-Gauge corrects the GSMaP-MVK value by increasing the amount of rainfall, leading to significant overestimations of accumulated rainfall and extremely high amounts of rainfall in May and June. This in turn causes a remarkably high FC and low K_2, which reduces the outflow formation (Fig. 4). Although GSMaP-MVK accumulations were marginally different from the rain gauge data (Fig. 3), their seasonal variation was drastically overestimated in June and moderately underestimated in the following months, but then the model performed well for the monthly rainfall during the first 5 months of the year (Fig. 4). This could be one of the factors that caused the parameter adjustments because of the bias in GSMaP-MVK rainfall to change the simulated discharge amount inconsistently (both increase and decrease) in the Upper-Cau river

basin. The excessively large FC and low K_2 resulted in a smaller discharge, while significantly lower BETA produced the larger stream flow (Fig. 10).

After blending the rain gauge data with the GSMaP-MVK, GSMaP-Gauge expressed a varied degree of improvements in terms of precipitation accumulations, monthly variation in rainfall, RMSE, and BIAS in the Hyeonsan, Fuji, and Da catchments. These improvements led to better parameter agreements with the observations for GSMaP-Gauge than for GSMaP-MVK in the Hyeonsan and Da catchments. However, in the Fuji catchment, the parameters obtained by GSMaP-Gauge input did not show as much similarity with the rain gauge data as in the Hyeonsan and Da catchments. Figure 9 shows that the recession coefficient of the lower reservoir K_2 of GSMaP-Gauge was dramatically less than that of the observation and GSMaP-MVK. This was partly due to the different trends than the ground measurements in the seasonal variation in the rainfall budget in GSMaP-Gauge (Fig. 4b). GSMaP-Gauge overestimated the monthly water amount during the rainy season and underestimated monthly water budget during the dry season. During the wet season, some volume of water is kept in the in the lower layer tank and water is gradually released in dry season. The low GSMaP-Gauge K_2 value leads to reduction in lower tank outflow generation. This could be the result of significant surplus water budget during the rainy season. Similarly, the low GSMaP-Gauge K_2 value in Upper-Cau (Fig. 10) could be also the outcome of significant overestimates rainfall budget of GSMaP-Gauge (Fig. 4d). In the Upper-Cau river basin, as a result of enlarging the precipitation accumulations

Fig. 10 Box plots of 6 parameters impacting on generating discharge for calibration period 2002–2003 in Upper-Cau river basin
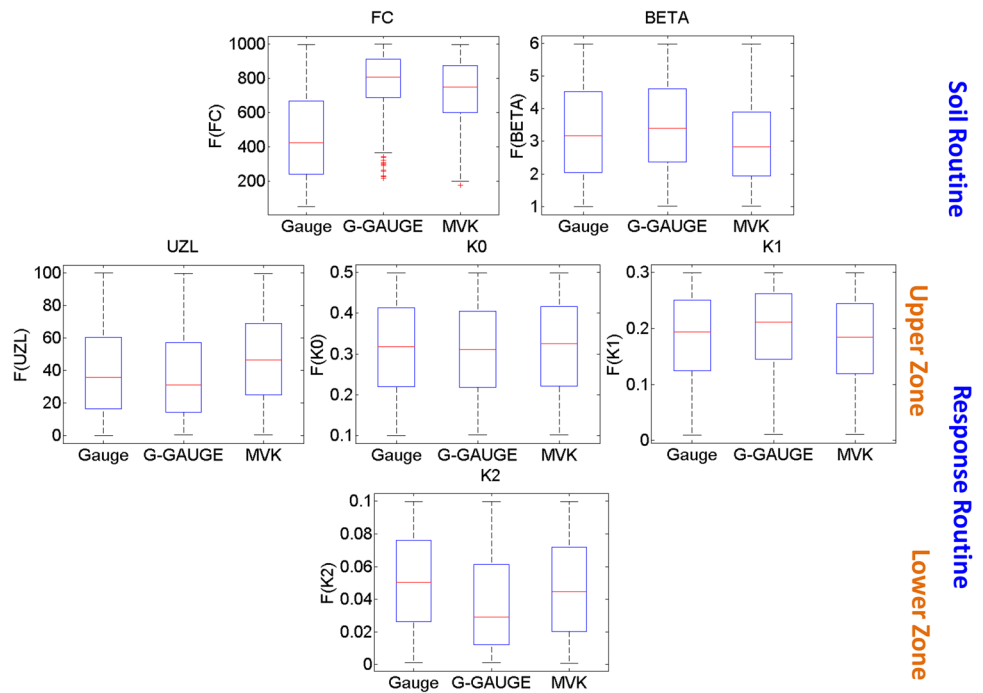

Fig. 11 Model performances **a** R^2 and **b** NS in 4 river basins of rainfall observations (green columns), GSMaP-Gauge (blue columns), and GSMaP-MVK (red columns) for calibration period
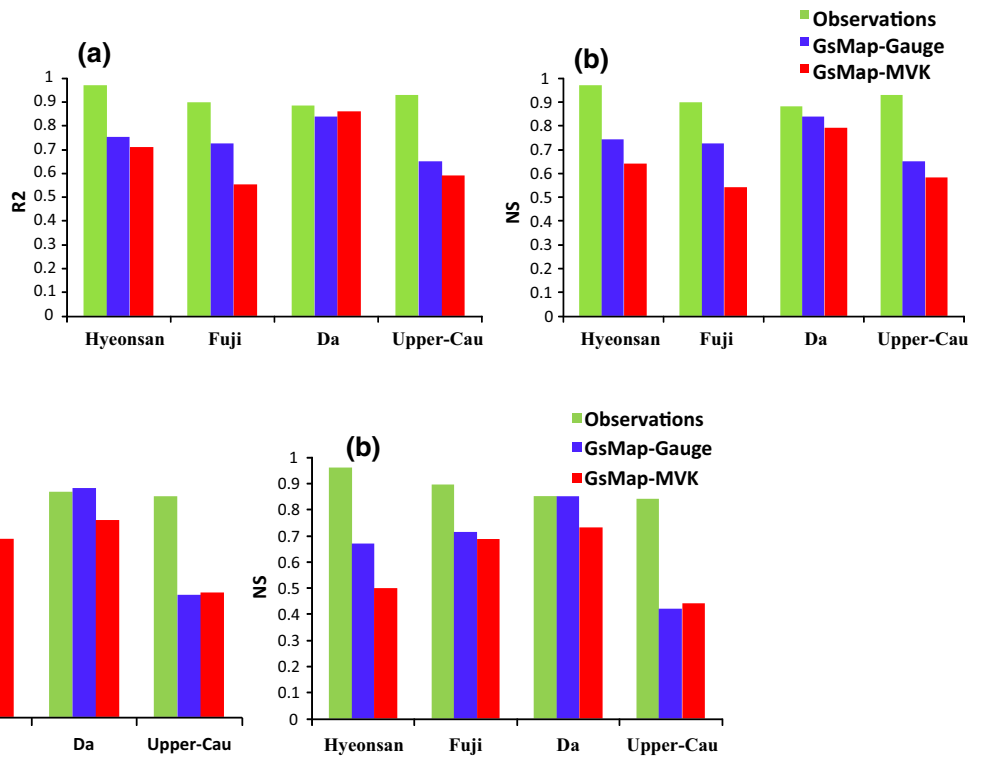

Fig. 12 Model performances R^2 and NS in 4 river basins of rainfall observations (green columns), GSMaP-Gauge (blue columns), and GSMaP-MVK (red columns) for validation period

RMSE and BIAS in the relationship with observed rainfall, GSMaP-Gauge did not enhance the parameter values to give values closer to the parameters retrieved from reference rain gauges.
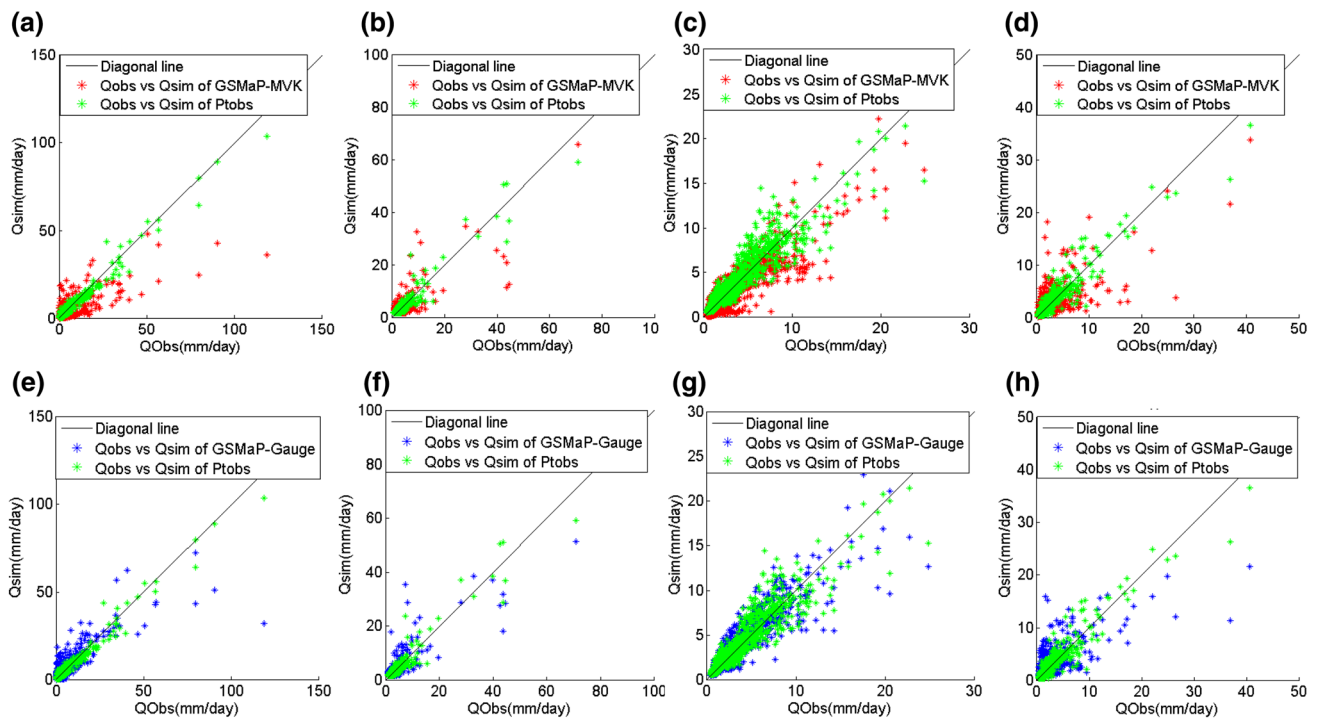
Fig. 13 Scatter plots between observed discharge and simulation discharge by rain gauge (green star) vs GSMaP-MVK (red star) and vs GSMaP-Gauge in **a**, **e** Hyeonsan, **b**, **f** Fuji, **c**, **g** Da and **d**, **h** Upper-Cau during the simulation period

Stream flow simulations using remote-sensing precipitation products

Figures 11 and 12 indicate the ability of the HBV model to simulate the discharge in the four targeted river basins with all of the model performances of the rainfall observations was larger than 0.7 for both the calibration and validation periods. An excellent fit was expressed in the Hyeonsan, Fuji, and Upper-Cau river basins, and there was a strong correlation in Da between the observations and simulated discharge (Fig. 13).

In the Hyeonsan river basin, GSMaP-MVK showed moderate simulation skill during the calibration period, with an N–S value of 0.64 and R^2 value of 0.71. However, there was a poor agreement between the observed and GSMaP-MVK simulated flows in this river basin with a low N–S value of 0.5 and R^2 of 0.52, respectively, during the validation period. It also expressed a tendency to substantially underestimate the high flow displayed in Figs. 13a and 14a. As a result of its better rainfall budget estimation and lower RMSE and BIAS, GSMaP-Gauge expressed a satisfactory performance, with a significant improvement by producing less underestimation of the high flow compared to the original GSMaP-MVK data (Figs. 13e and 14a). The R^2 values for the time series of daily simulated and observed discharge were 0.75 (for calibration) and 0.69 (for validation), and the N–S values were 0.74 and 0.67 for calibration and

validation, respectively, indicating that GSMaP-Gauge had reasonable skills in reproducing stream flow in the Hyeonsan catchment.

In the Fuji catchment, although GSMaP-MVK simulated the stream flow with moderate skill, with intermediate N–S and R^2 values (0.54 and 0.55, respectively) during calibration, it had an acceptable performance during validation with N–S and R^2 values larger than 0.65. When GSMaP-MVK was replaced by GSMaP-Gauge, the model calibration performance produced a remarkable increase of approximately 24% for both N–S and R^2, and a modest improvement of 5% for R^2 and 4% for N–S during validation. These results indicate a fair skill of GSMaP-Gauge for simulations reproducing discharges measured on the ground.

In the Da river basin, GSMaP-MVK displayed satisfactory model performance, with N–S and R^2 values of 0.86 and 0.79 during calibration and 0.76 and 0.73 during validation, respectively. However, as shown in Fig. 14c, there were significant underestimations for GSMaP-MVK, particularly during the low-flow period. In contrast, the flow estimated from GSMaP-Gauge matched the observed pattern of discharge shown in Fig. 14c quite well and expressed satisfactory skill for stream flow simulations, with the model performances larger than 0.84 for both the validation and calibration phases.

In the Upper-Cau river basin, both GSMaP-MVK and GSMaP-Gauge expressed the weakest simulation skills of
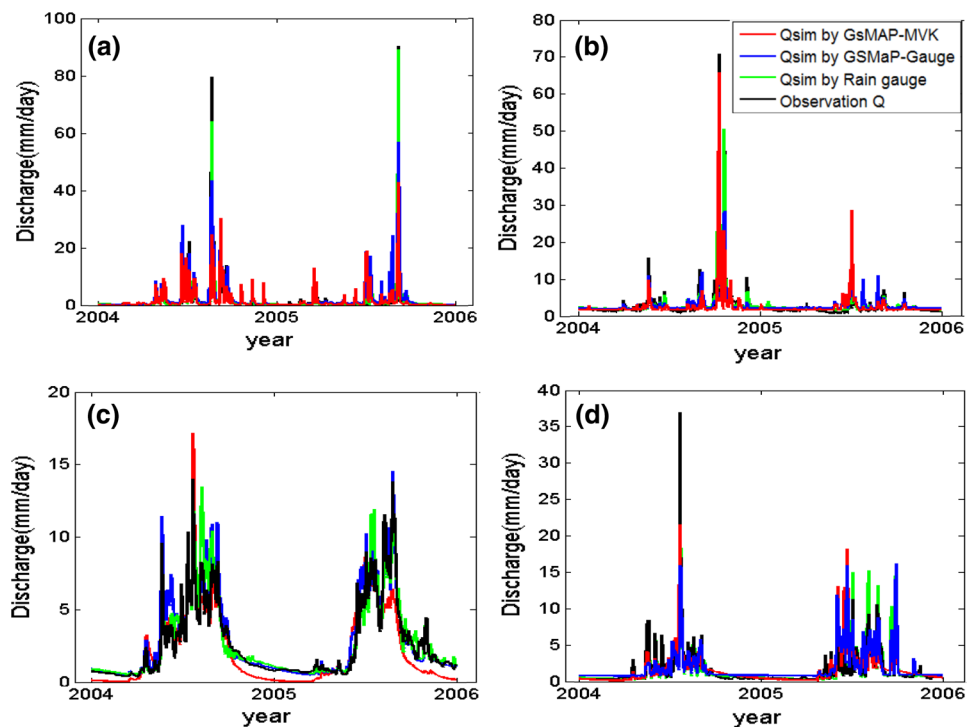
all four study areas. Figure 13d, h shows the underestimation of high flow (larger than 20 mm/day) for both GSMaP-Gauge and GSMaP-MVK. These underestimations can be observed in a hydrograph of the Upper-Cau river basin in Fig. 14d. In Fig. 12, the low R^2 values (0.47 and 0.48) for GSMaP-Gauge and GSMaP-MVK, respectively, and low N–S values (consistently <0.45) indicate that the reproduction of discharge by these two satellite-based precipitation products was not satisfactory. It should be noted that the R^2 and N–S values of GSMaP-Gauge were even worse than those of GSMaP-MVK, as shown by the larger RMSE and BIAS values (Table 3). This is probably due to either the lower number of rain gauges used for adjusted gauge data in this river basin or a limitation of the GSMaP-Gauge blending algorithm itself.

Discussion and conclusions

Two remote-sensing precipitation products, GSMaP-Gauge and GSMaP-MVK, were investigated to determine the effectiveness of combining rain gauge data with satellite-only products to enhance their rainfall estimation performances. The suitability of these two global products as an input for the conceptual model HBV was also investigated, to simulate the daily stream flow in several river basins located in areas with various degrees of complex topography, under varied climate conditions.

It was interesting that the gauge–satellite product produced remarkable improvements in model performance compared to the satellite-only precipitation data in both temperate basins (Hyeonsan and Fuji) and a subtropical basin (Da). In those catchments, GSMaP-Gauge performed moderately satisfactory to well when reproducing discharge, with N–S and R^2 values consistently higher than 0.65 for both validation and calibration (Figs. 11 and 12). This indicates the success of adjusting GSMaP-MVK using CPC global gauge data to generate GSMaP-Gauge in these areas. However, because of substantial overestimations of the rainfall amount and the increase in RMSE and BIAS, GSMaP-Gauge slightly worsened the performance of GSMaP-MVK in the Upper-Cau river basin. This indicates the need to modify the GSMaP-Gauge retrieval algorithm for blending gauge and satellite information due to the data limitations of sparse rain gauge networks.

Due to the uncertainties in the rainfall estimates of remote-sensing precipitation products, the parameters were adapted in such a way that the model produced more stream flow. Although GSMaP-MVK significantly and continuously underestimated the rainfall accumulations and monthly seasonal variation in the Hyeonsan and Da river basins, GSMaP-Gauge resulted in dramatic improvements in terms of these two aspects. Therefore, these improvements led to better parameter agreements with the observations of GSMaP-Gauge than those of GSMaP-MVK in these basins. However, in the Fuji river basin, the parameters obtained by GSMaP-Gauge input were not as similar to the rain gauge

data as in the Hyeonsan and Da basins. This was partly due to the different trends with the ground measurements in the seasonal variation in the rainfall budget in GSMaP-Gauge. In the Upper-Cau, as a result of the increased precipitation accumulations, RMSE, and BIAS in the relationship with observed rainfall, GSMaP-Gauge did not enhance the parameter values to give a value closer to the parameters retrieved from reference rain gauges.

Significant rainfall underestimations in the Hyeonsan, Fuji, and Da river basins (Figs. 3 and 4) and the poor relationship with rain gauge data in the monthly rainfall budget in the Upper-Cau river basin (Fig. 4) can be partly ascribed to an orographic effect. This leads to GSMaP-MVK displaying poor to moderately satisfactory discharge simulation skills in those four river basins. Therefore, the accuracy of GSMaP-MVK needs to be further improved to become a more effectively useable product for hydrological simulation.

References

Aonashi K, Shibata A, Liu G (1996) An over-ocean precipitation retrieval using SSM/I multi-channel brightness temperature. J Meteorol Soc Jpn 74:617–637

Bitew MM, Gebremichael M (2010) Assessment of satellite rainfall products for stream-flow simulation in medium watersheds of the Ethiopian Highlands. J Hydrol Earth Syst Sci 15:1147–1155

Bitew MM, Gebremichael M, Ghebremichael LT, Bayissa YA (2012) Evaluation of high-resolution satellite rainfall products through streamflow simulation in a hydrological modeling of a small mountainous watershed in ethiopia. J Hydrometeorol 13:338–350

Dinku T, Connor SJ, Ceccato P (2010) Comparison of CMORPH and TRMM-3B42 over mountainous regions of Africa and South America. J Satellite Rainfall Appl Surf Hydrol:193–304

Hsu K, Gao X, Sorooshian S, Gupta HV (1997) Precipitation estimation from remotely sensed information using artificial. J Appl Meteorol 36:1176–1190

Huffman GJ, Bolvin DT, Nelkin EJ, Wolff DB, Adler RF, Gu G, Hong Y, Bowman KP, Stocker EF (2007) The TRMM Multisatellite Precipitation Analysis (TMPA): quasi-global, multiyear, combined-sensor precipitation estimates at fine scales. J Hydrometeorol 1(8):38–55

Jayawardena AW, Takeuchi K, Machbub B (1997) Catalogue of river for Southeast Asia and the Pacific. A UNESCO-IHP Publications, Paris

Jayawardena AW, Takeuchi K, Machbub B (2002) Catalogue of river for Southeast Asia and the Pacific IV. A UNESCO-IHP Publications, Paris

Jayawardena AW, Takeuchi K, Machbub B (2012) Catalogue of river for Southeast Asia and the Pacific VI. A UNESCO-IHP Publications, Paris

Joyce RJ, Janowiak JE, Arkin PA, Xie PP (2004) Cmorph: a method that produces global precipitation estimates from passive microwave and infrared data at high spatial and temporal resolution. J Hydrometeorol 5:487–503

Kendale BM (2011) 1970-73 Drought of Maharashtra with special reference to state and legislative response. Department of History Shri Shiv Chhatrapati College Junnar Pune, Pune

Kubota T, Shige S, Hashizume H, Aonashi K, Takahashi N, Seto S, Hirose M, Takayabu Y, Nakagawa K, Iwanami K, Ushio T, Okamoto K (2007) Global precipitation map using satellite-borne microwave radiometers by the GSMaP project: production and validation. IEEE Trans Geosci Remote Sens 45:2259–2275

Liu X, Yang T, Hsu K, Liu C, Sorooshian S (2017) Evaluating the streamflow simulation capability of PERSIANN-CDR daily rainfall products in two river basins on the Tibetan Plateau. J Hydrol Earth Syst Sci 21:169–181

Nibret AA, Fred LO, Nawa RP (2010) Sensitivity and uncertainty analysis of conceptual HBV rainfall-runoff model: implication for parameter estimation. J Hydrol 398:301–310

Seibert J (2005) HBV light. Version 2. User's manual, Stockholm

Shrestha MS, Artan GA, Bajracharya SR, Sharma RR (2008) Using satellite-based rainfall estimation for stream-flow modeling: Bagmati Basin. J Flood Risk Manag 1(2):88–99

Stisen S, Sandholt I (2010) Evaluation of remote-sensing-based rainfall products through predictive capability in hydrological runoff modeling. J Hydrol Process 24:879–891

Su F, Hong Y, Lettenmaier DP (2007) Evaluation of TRMM Multisatellite Precipitation Analysis (TMPA) and its utility in hydrologic prediction in the La Plata basin. J Hydrometeorol 9:622–640

Thai TH, Thao NP, Dieu BT (2017) Assessment and simulation of impacts of climate change on erosion and water flow by using the soil and water assessment tool and GIS: Case Study in Upper Cau River basin in Vietnam. Vietnam J Earth Sci 39:376–392

Tobin KJ, Bennett ME (2009) Using SWAT to model streamflow in two river basins with ground and satellite precipitation data. J Am Water Resour Assoc 45:253–271

Ushio T, Kubota T, Shige S, Okamoto K, Aonashi K, Inoue T, Takahashi N, Kachi K, Oki R, Morimoto T, Kawasaki Z (2009) A Kalman filter approach to the Global Satellite Mapping of Precipitation (GSMaP) from combined passive microwave and infrared radiometric data. J Meteorol Soc Jpn 87A:137–151

Ushio T, Tashima T, Kubota T, Kachi M (2013) Gauge Adjusted Global Satellite Mapping of Precipitation (GSMaP_Gauge)

Xu CY, Vandewiele G (1994) Sensitivity of monthly rainfall-runoff models to input errors and data length. J Hydrol Sci 39(2):157–176

Yilmaz KK, Hogue TS, Hsu K-L, Sorooshian S, Gupta HV, Wagener T (2005) Intercomparison of rain gauge, radar, and satellite-based precipitation estimates with emphasis on hydrologic forecasting. J Hydrometeorol 6:497–517